



Design and Performance Evaluation of a 6×6 MIMO Array with Partial Ground Plane for Sub-6 GHz Mobile Applications

Fahmida Hossain¹ A. K. M. Zakir Hossain^{1*} Muhammad Ibn Ibrahimy²
 Jamil Abedalrahim Jamil Alsayaydeh¹

¹*Fakulti Teknologi dan Kejuruteraan Elektronik dan Komputer (FTKEK),
 Universiti Teknikal Malaysia Melaka (UTeM), Melaka, Malaysia*

²*Faculty of Engineering, Dept. of Electrical and Computer Engineering (ECE),
 International Islamic University Malaysia (IIUM), Gombak, Malaysia*

* Corresponding author's Email: zakir@utem.edu.my

Abstract: This article presents a 6×6 MIMO array optimized for sub-6 GHz mobile and wireless applications. Utilizing a partial ground plane (PGP), the array incorporates a single-element half-circle-slotted monopole antenna to achieve a wideband response. The compact design, measuring 75 × 150 mm² and only 0.508 mm thick, is engineered to fit 6.6-inch display smartphones. Operating between 2.82 and 5.95 GHz, the array offers a -10 dB bandwidth and a VSWR of less than 2. It also delivers port-to-port isolation less than -20 dB and a peak realized gain of 5.3 dBi, with an antenna efficiency of 71%. Comprehensive far-field radiation patterns are observed across all 6 ports. The array maintains an envelope correlation coefficient (ECC) under 0.004 and a diversity gain (DG) above 9.98, demonstrating robust performance. Specific absorption rate (SAR) results at 3.5 GHz confirms compliance with MIMO standards, with values as low as 0.13 W/kg. This high-performance MIMO array is a strong contender for sub-6 GHz 5G applications.

Keywords: MIMO array, Sub-6 GHz, Partial ground plane (PGP), Wideband antenna, Smartphone integration.

1. Introduction

In the ever-evolving path of wireless communication, 5G technology has emerged as a groundbreaking solution for many previous problems associated with 4G. Its introduction signifies a leap, offering an array of benefits, including substantially reduced latency, vastly improved connectivity, faster data transfer rates, and remarkable high-speed capabilities [1]. What makes 5G even more intriguing is its ability to operate across an array of distinct frequency bands, serving as a testament to the global adoption of this transformative technology.

5G frequency bands in the realm of wireless communication can be broadly divided into two main categories. The first category is the sub-6 GHz band, also known as FR1, which spans from 450 MHz to 6000 MHz. The second category is the

millimeter-wave (mmWave) band, referred to as FR2, which covers the range from 24.25 GHz to 52.6 GHz. Specific frequencies of significance within the sub-6 GHz band include 700 MHz, often referred to as the lower band, the 3.4-3.6 GHz range, which constitutes the mid-band, and the 4.8-6 GHz range, known as the high band [2].

The widespread adoption of these 5G frequency bands by countries across the globe has given rise to a unique challenge – the need to reengineer essential hardware components of wireless cellular communication systems. Among these components, base transceiver stations (BTS) and mobile handsets must undergo significant modifications to accommodate the specific frequency requirements dictated by different nations. In this sophisticated scenario of wireless communication, the antenna emerges as a linchpin, serving as the primary gateway device responsible for transmitting and

receiving signals [2]. To effectively meet the demands of 5G communication, meticulous design and engineering of antenna arrays become paramount. This holds true for both ends of the communication spectrum – the base station and the mobile station. When it comes to devising MIMO (multiple-input multiple-output) antenna arrays for mobile devices, a difficult challenge arises in fitting these arrays within the often limited in space available in mobile devices. It has been observed that the MIMO antennas intended for sub-6 GHz 5G smartphones can be classified according to four essential factors: how they operate, the quantity of antenna elements they include, whether they utilize isolation circuitry, and the specific arrangement of the antenna structure. Consequently, crafting a MIMO array that strikes the delicate balance between a limited number of elements, high bandwidth (BW), minimal isolation, and a straightforward structural design becomes a formidable task that both scholars and antenna engineers grapple with.

One promising solution for 5G smartphones involves implementing a reconfigurable MIMO array featuring two antenna elements. In this proposed design, each antenna element comprises two meander line radiating arms that can be automatically connected or disconnected from the 50Ω feedline. This capability introduces valuable frequency diversity, enabling operation at either 2.4 GHz or 3.5 GHz frequencies. Remarkably, at these frequencies, the envelope correlation coefficient (ECC) measures 0.0056 and 0.0009, respectively, underscoring the effectiveness of this design. However, this antenna array achieves a very low minimum isolation level of 12 dB and of course works in limited capacity [3].

Another study [4] introduces a dual-element MIMO array specially designed for smartphones. This particular antenna boasts a good coverage range, spanning over 400 MHz across two mid sub-6 GHz bands – precisely, 3.5 GHz and 4.3 GHz. Its capabilities extend even further, encompassing frequencies up to 12 GHz within the mmWave 5G bands, which operate between 24 GHz and 38 GHz. The sub-6 GHz bands achieve a substantial minimum isolation level of 21 dB, while the mmWave bands reach an impressive isolation of 24 dB. These achievements are realized through the strategic utilization of complementary metamaterial unit cells positioned between the two antenna elements. Importantly, the ECC for this advanced antenna array remains consistently below 0.05.

The prevalence of four-port MIMO antenna arrays is gaining momentum within both research

and industry circles, particularly concerning 5G smartphones, given their exceptional performance capabilities[5]. In [6], a four-element dual-band MIMO array is meticulously developed for integration into 5G mobile terminals using side edge positioning technique. This array effectively operates within two distinct frequency ranges: 3.4 GHz to 3.6 GHz and 4.8 GHz to 5.0 GHz, showcasing an impressive isolation level as low as -17.5 dB. However, this array demonstrates a low total efficiency (TE) of only 60% and an ECC below 0.05 across both frequency bands.

Another proposal is presented in [7], featuring a 2×2 MIMO array with a quad-port dual-band configuration. This array functions good with 200 MHz bandwidths, spanning frequencies from 3.4 GHz to 3.6 GHz and 4.8 GHz to 5.0 GHz. However, its performance gets curtailed as it can achieve a TE of 70% only. Even though the authors used the parasitic rectangle strip to enhance the isolation but could not achieve more than a level of 16.5 dB. Yet another approach is introduced in [8] utilizing the space and pattern diversity, where a four-element MIMO dipole array is proposed for 5G handsets, boasting dual-band capability and dual diversity. This array showcases an ECC as low as 0.005, however, dents its performance as the minimum isolation level goes as low as -15 dB only. Again, the TE is only 51% at port 1 antenna. Additionally, the paper provides a good SAR analysis, examining the interaction of the array with the human head and hand and result is 1.7W/Kg at 3.5GHz.

In recent times the researchers have also made several approaches to propose innovative designs consisting of six [9], eight [10-13], ten [14] and twelve [15, 16] element MIMO array antennas to improve the parameter of MIMO for mobile phone for sub-6 GHz (5G) communications. In [9], the authors have proposed a six-element MIMO array that operates below 2.5 GHz. They employed a slotted technique to achieve resonance and incorporated parasitic elements between the antennas to enhance isolation. Additionally, a modified ground structure was utilized to improve MIMO performance. However, the results indicate that, while the measured isolation reaches a minimum of 45 dB, the maximum isolation only degrades to -12 dB. Furthermore, although the array is intended for mobile phone applications, no specific SAR analysis has been presented for this technique.

In [10], an eight-element (8×8) array designed for the 3.5 GHz 5G band on an FR4 substrate. This design employs a modified and rectangular-slotted ground plane, with antennas placed side by side for

a MIMO configuration suitable for smartphones. Small rectangular slots separate the antennas. The s -parameter results indicate an in-band resonance dip as low as -28 dB and an ECC of 0.03, meeting acceptable standards. However, isolation remains as a challenge, barely reaching -12 dB, and again, there is no SAR analysis presented for smartphone applications. Similarly, a new proposal is made by utilizing the dual polarized self-complementary antennas (SCA) with the edge corner probe-feed technique at 3.6 GHz [11]. With this technique the array produces a high-gain pattern, improved radiation coverage and low ECC level of 0.004 in simulation. Also, the SAR value for the Antenna 3 is 1.8 W/Kg which is within the acceptable range. Yet, the isolation between port 1 and 2 (S_{21}) is not so good, achieving only less than -12dB and measured ECC is surprisingly high around 2 shows the limitation of this design.

In [12], an 8-element MIMO array design for 5G smartphones uses deep learning (DL) for efficient antenna dimension estimation, bypassing traditional electromagnetic simulation. Nevertheless, the chosen -6 dB bandwidth might lead to significant circuit-side reflection. Its isolation, peaking at -12.5dB, falls short of the -15dB benchmark. The omission of SAR analysis hinders evaluating its suitability for smartphone use. Similarly, [13] presents an 8-element array operating between 3.6-4.7 GHz, characterized by an open L-slot on the ground plane and a coaxial feed L-shaped radiating element. This structure yields a favorable ECC of 0.08 and TE ranging from 87-96%. However, the same -6dB bandwidth may induce port reflections, and the port-to-port isolation is suboptimal, barely reaching -11dB.

In [14], a 10-element array is proposed. The array utilizes the slotted GP technique to achieve the desired resonance and the isolation between the ports for sub-6 GHz bands. 10 different antennas are placed side by side in parallel to produce the MIMO configuration for the smart phones. The array has achieved a good peak SAR value of 1.28 W/Kg for 1-g tissue with 25mW input power. The array also has a good ECC of 0.07. However, the port-to-port results show that it has a mere -11dB isolation which is low in terms of the standard in MIMO technique. Also, the TE drops to 65% with this technique.

Reaching for higher element in [15, 16], the authors have proposed 12-element MIMO array both for 5G smart phones at 3.5GHz. Both proposals use side edge positioning technique to gain advantage on MIMO performances. In [15] the authors use open loop single element antenna with remarkably

Table 1. Comparison between existing works with proposed work

Ref	Technique Used	Isolation (dB)	ECC	SAR, W/Kg	TE (%)
[4]	Metamaterial unit cells	-21	0.05	Na	50
[6]	Side edge positioning	-17.5	0.05	Na	60
[7]	Parasitic rectangle strip	-16.5	0.01	Na	70
[8]	Space and pattern diversity	-15	0.005	1.7	51
[9]	Parasitic patch and slotted GP	-12	0.002	Na	88
[10]	Slotted GP	-12	0.03	Na	70
[11]	Edge corner probe-feed	-12	0.004	1.8	70
[12]	DL	-12.5	0.1	Na	Na
[13]	L-slotted GP	-11	0.08	Na	87
[14]	Slotted GP	-11	0.07	1.28	65
[15]	Side edge positioning	-12	0.42	Na	39
[16]	Side edge positioning	-10	0.4	Na	36
This work	PGP and 90° sequentially rotation	-20	0.004	0.78	71

Na = Not available

small dimension of $5.85 \times 4.9 \text{ mm}^2$ to make it a very compact size. However, to do so, the array suffered a low isolation on only -12dB and the TE also decreased to as low as 39%. Also, the ECC is high about 0.42 and the peak gain is as low as 3.2dBi only. Similarly, it can be seen from the results in [16] that the array has only -10dB of lowest isolation, the ECC is higher than 0.4 at 3.5GHz and the TE drops to 36% only. Furthermore, in both of these 12-element MIMO designs no SAR analysis is presented. Table 1 summaries the performances parameter along with used techniques.

It is evident from these available previous proposals (in Table 1) that some of the work performs well in certain performance parameters, while others do not. Some designs exhibit good isolation but show limitations in ECC or efficiency parameters and so on. Additionally, many proposals are intended for implementation in smartphones, yet no adequate SAR analysis is presented. Addressing these issues within the context of this article, we propose the design and development of a 6×6 element MIMO array featuring a modified rectangular monopole antenna configuration with three half-circular slots. The PGP technique is

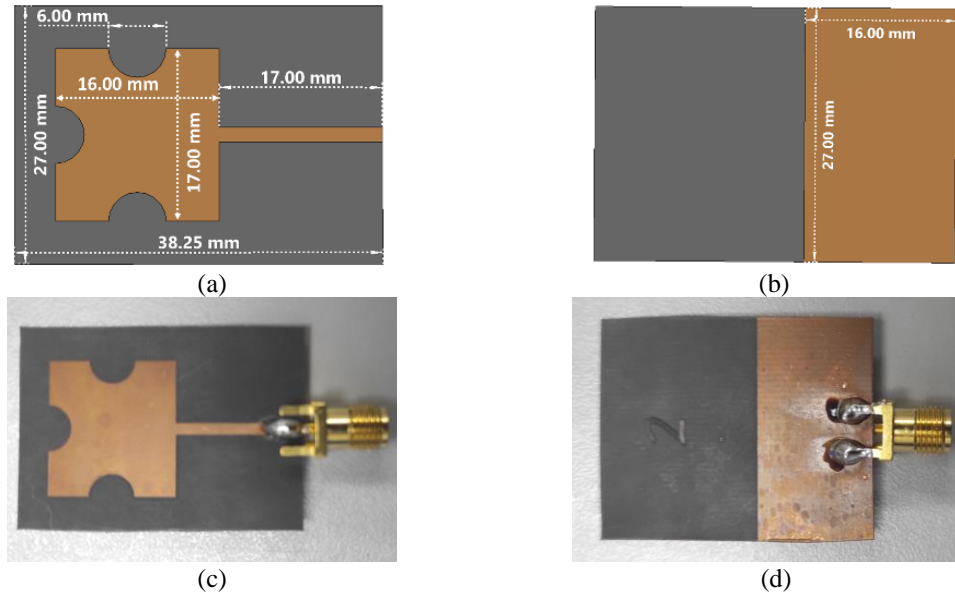


Figure. 1 SEA design and layout: (a) SEA front layout, (b) SEA back layout, (c) SEA front (fabricated), and (d) SEA back (fabricated)

employed to achieve resonance and ultra-wideband performance. Moreover, the sequential rotation of 90 degrees between the ports is utilized to attain high isolation within the BW. By leveraging these techniques, we have produced a MIMO array with improved isolation, very low ECC and SAR, and high efficiency. The subsequent sections of this article (section 2) delve into the design and synthesis of both the single element antenna (SEA) and the 6-element (6×6) MIMO. Section 3 provides an in-depth exploration of the performance characteristics of these antenna configurations, accompanied by relevant graphical representations. The article concludes in section 4 with a summary of the proposed work.

2. Design of single antenna (SEA) and MIMO array

Fig. 1 illustrates the proposed single element antenna (SEA) layout along with its dimensions. The design and simulation of the antenna were performed using CST MWS 2022. Figs. 1(a) and 1(b) show the front and back views of the SEA in the simulation, respectively. Similarly, Figs. 1(c) and 1(d) reveal the fabricated front and back views of the design. The substrate used here is Rogers RT Duroid 5880 with the dielectric constant ($\epsilon_r = 2.2$) and the dissipation factor ($\tan\delta$) of 0.0009 and it has been fabricated by etching technique. The SEA consists of a rectangular patch, a transmission line connected to the feed, and three half-circular slots of equal size inserted into the top, right, and left sides of the patch. The center of each half-circular slot aligns with the midpoint of its respective side. The

dimensions of the rectangular patch (length and width) and the radii of the slots are estimated by Eqs. (1), (2), and (3), respectively and later optimized in CST MWS [17]. Where, C_0 is the speed of light, ϵ_r & ϵ_e are the relative and effective dielectric constant of the substrate, h is the height of the substrate, f_c is the resonant frequency, and $F = \frac{8.791 \times 10^9}{f_c \sqrt{\epsilon_r}}$. Hence the final length (L), width (W) and the radius (r) of the half-circular slot are obtained as 17 mm, 16 mm, and 6 mm respectively for the patch.

$$W = \frac{C_0}{2f_c \sqrt{\frac{\epsilon_r + 1}{2}}} \quad (1)$$

$$L = \frac{C_0}{2f_c \sqrt{\epsilon_e}} - 0.824h \frac{(\epsilon_e + 0.3) \left(\frac{W}{h}\right)^k + 0.264}{(\epsilon_e - 0.258) \left(\frac{W}{h}\right)^k + 0.8} \quad (2)$$

$$r = \frac{F}{\left\{1 + \frac{2h}{\pi \epsilon_r F} \left[\ln\left(\frac{\pi F}{2h}\right) + 1.7726 \right] \right\}^{\frac{1}{2}}} \quad (3)$$

Also, the microstrip feedline length is kept the same as the width of the antenna. Again, the final dimension of the antenna is obtained as $27 \times 38.25 \text{ mm}^2$ after optimizing in CST MWS.

Fig. 2 illustrates the progressive stages of the antenna's design. The process began with a fundamental rectangular microstrip patch antenna, complete with a full ground plane (GP). Subsequently, in the second phase, three half-circular slots were integrated while preserving the full GP. The design culminated in the third stage with the introduction of a partial ground plane

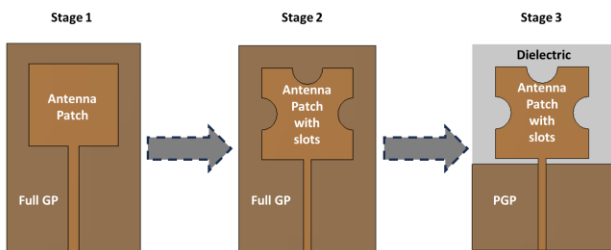


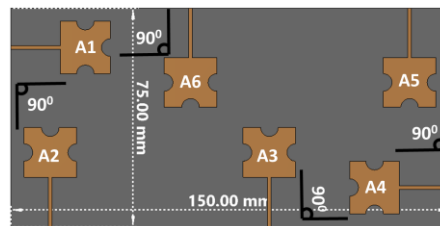
Figure. 2 Layout for different stages of single element antenna design

(PGP), fine-tuned to secure the target operational frequency within the sub-6 GHz spectrum. A comprehensive explanation with s-parameter results of this process is provided in the results and discussion section (section 3).

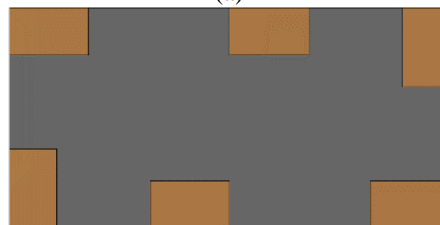
Fig. 3 provides a comprehensive view of our 6×6 MIMO antenna design. Figs. 3(a) and 3(b) offer detailed front and back views of this design. Notably, the dimensions of the design are carefully tailored, with a length of 150 mm and a width of 75 mm, closely mirroring the size of a standard 6.6-inch smartphone. Each of the six antennas, denoted as A1-A6 respectively, is sequentially positioned to optimize performance. To achieve minimal interference and crosstalk between ports, we've employed a sequential rotation technique, ensuring that adjacent ports are precisely 90 degrees apart in polarization [17]. Linear polarization can be either horizontal or vertical. For optimal transmission and reception, the transmitting (Tx) and receiving (Rx) antennas must have matching polarization. Mismatches in polarization can result in loss at the Rx side. Specifically, if a vertically polarized antenna is at the Rx side and a horizontally polarized antenna is at the Tx side (or vice versa), there theoretically will be no communication between them. In MIMO systems, a 90-degree polarization mismatch between adjacent ports produces a similar effect by guaranteeing a (theoretical) zero crosstalk between the ports, enhancing the overall efficiency and reliability of the MIMO system [18].

In addition to managing isolation using polarization technique between adjacent ports, we have taken measures to prevent isolation issues between other antenna pairs. Specifically, antennas A3 and A4, as well as A5 and A6, operate at the same polarization. To mitigate any potential isolation problems, we have maintained 90 mm between these antenna pairs.

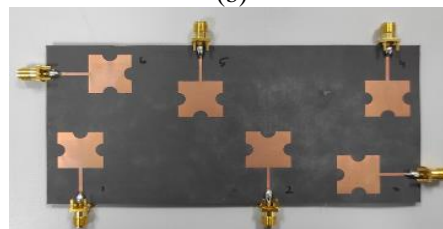
Fig. 3(d) showcases the fabricated prototype, offering a representation of our design's front and back views. Finally, Fig. 3(e) reveals the setup employed to calculate the SAR of the design—a



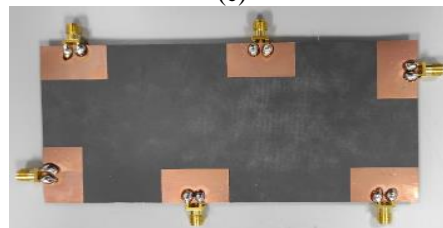
(a)



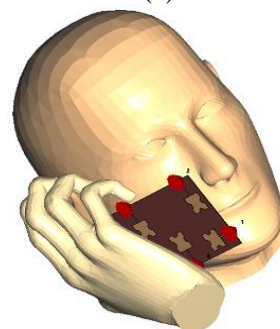
(b)



(c)



(d)



(e)

Figure. 3 (a) - (d) MIMO design layouts and (e) SAR setup with hand-head phantom: (a) 6×6 MIMO front view, (b) 6×6 MIMO back view, (c) 6×6 MIMO front view (fabricated), and (d) 6×6 MIMO back view (fabricated), and (e) SAR simulation setup with hand-head phantom in CST

critical consideration for smartphone applications. SAR assessment ensures that the antenna design meets safety standards and does not expose users to excessive radiofrequency. The input power is considered as 50mW (17dBm) for this calculation. Next section (III) reveals the detailed results with an in-depth discussion for both SEA and 6×6 MIMO

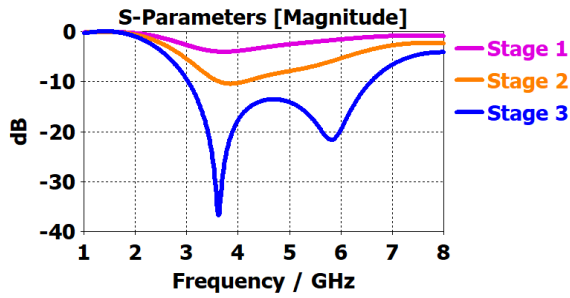


Figure. 4 S11 response of different stages of SEA design design.

3. Results and discussions

Fig. 4 displays the S11 responses at various stages of the SEA design depicted in Fig. 2. At stage 1, featuring a basic rectangular patch and a full GP, the S11 result does not cross the -10dB threshold, indicating an absence of resonance. In stage 2, the introduction of three half-circular slots (retaining the full GP) initiates a descent in the S11 value, approaching -10dB, yet not surpassing this mark. At stage 3, the modification to a PGP result in resonance at 3 GHz, extending beyond 6.5GHz, with the deepest dip of -37dB observed at 3.55 GHz making it an ultra-wide band response proving the usefulness of the PGP in this design.

Next, Fig. 5 illustrates different impedances, s-parameter, VSWR and the 3-D & 2-D radiation pattern responses. From Fig. 5 (a) it is seen that the reference impedance is accurately at 50Ω . It means the feed of the antenna is matched perfectly for 50Ω SMA connectors in simulation. Similarly, it is seen from Fig. 5(b) is at 3.5GHz the antenna has a zero imaginary impedance along with a 50Ω real value ($Z_{ant} = 50 + j0 \Omega$). This also indicates the low loss nature of the design. Figs. 5 (c) and 5 (d) reveal the measured and the simulated S₁₁ and VSWR characteristics of the SEA design respectively, and these measurements were conducted using a vector network analyzer (VNA) with the model number Agilent N5242A. In Fig. 5(c), it is evident that the measured and simulated results of S₁₁ exhibit a commendable level of agreement. However, a slight shift has been observed, attributable to variations in fabrication quality and SMA soldering. Analyzing the simulated S₁₁ results, it is apparent that the operational bandwidth initiates at 3.00 GHz and extends up to 6.5 GHz, yielding a bandwidth of 3.5 GHz. However, the measured results indicate a slightly reduced bandwidth, spanning from 2.8 GHz to 5.9 GHz, equivalent to a bandwidth of 3.1 GHz. Nevertheless, it is noteworthy that the bandwidth reduction amounts to merely 400 MHz, preserving most of the band.

Furthermore, a check of the VSWR responses, both measured and simulated, reveals a shift of approximately 370 MHz. Consequently, it can be concluded that the effective operational bandwidth of this SEA spans from 2.82 GHz to 5.95 GHz, totaling 3.13 GHz. These results underscore the antenna's robust performance within this frequency range. Moreover, Figs. 5(e)-5(f) illustrates the radiation characteristic of the SEA. Fig. 4(e) reveals the 3-D radiation pattern response at 3.5GHz and it is seen that the radiation plane is mostly on x-y plane which proves the omni-direction pattern of the antenna. Fig. 5(f) reveals the 2-D $\phi = 0$ and $\phi = 90$ radiation patterns which also supports the omni-directional nature of the SEA design.

Moving on to the responses for the 6×6 MIMO design, Fig. 6 reveals both the measured (M) and the simulated (S) responses of the S-parameters between the ports. In any MIMO design, the S-parameters between the ports are considered indicative of the isolation between them. For example, the S₂₁ response, chosen due to the symmetry of the design, implies the isolation between port 1 and port 2, and so on.

This figure comprises the measurement setup (Figs. 6 (a) and 6 (b)) and the s-parameter responses (Figs. 6 (c) and 6 (d)) to analyze the isolation performance of the designed MIMO array. Fig. 6(c) comprises the responses of S₂₁, S₃₁, S₄₁, S₅₁, and S₆₁, indicating the isolation of port 1 with the other 5 ports. It is evident that the measured and simulated responses are in excellent agreement.

Most of the responses are below the -20 dB level. However, we observe that for S₂₁(M), within the narrow band of 2.76 – 3.2 GHz, the value reaches as high as -16.4 dB, but it falls below -20 dB from 3.2 GHz until the end of the BW. Considering that the standard minimum isolation is ≤ -15 dB between any ports of the MIMO design [19], we can conclude that the response still complies well with the standard. Fig. 6(d) shows the isolation between port 2 and the other ports, also revealing the isolation between port 3 and port 4 (S₄₃). Notably, only S₆₂ falls within the -20 dB to -30 dB range, while the rest exhibit isolation levels below -30 dB. This demonstrates the high quality of the design.

A similar scenario can be observed in Fig. 6(e), which comprises the isolation responses between port 4 & port 5 (S₄₅), port 5 & port 3 (S₅₃), port 6 & port 3 (S₆₃), and port 6 & port 5 (S₆₅), where all the isolation values between ports remain below -26.4 dB. In summary, we can confidently state that the isolation performance of this design is highly satisfactory. Two additional parameters, ECC and DG of the MIMO, have been calculated using CST

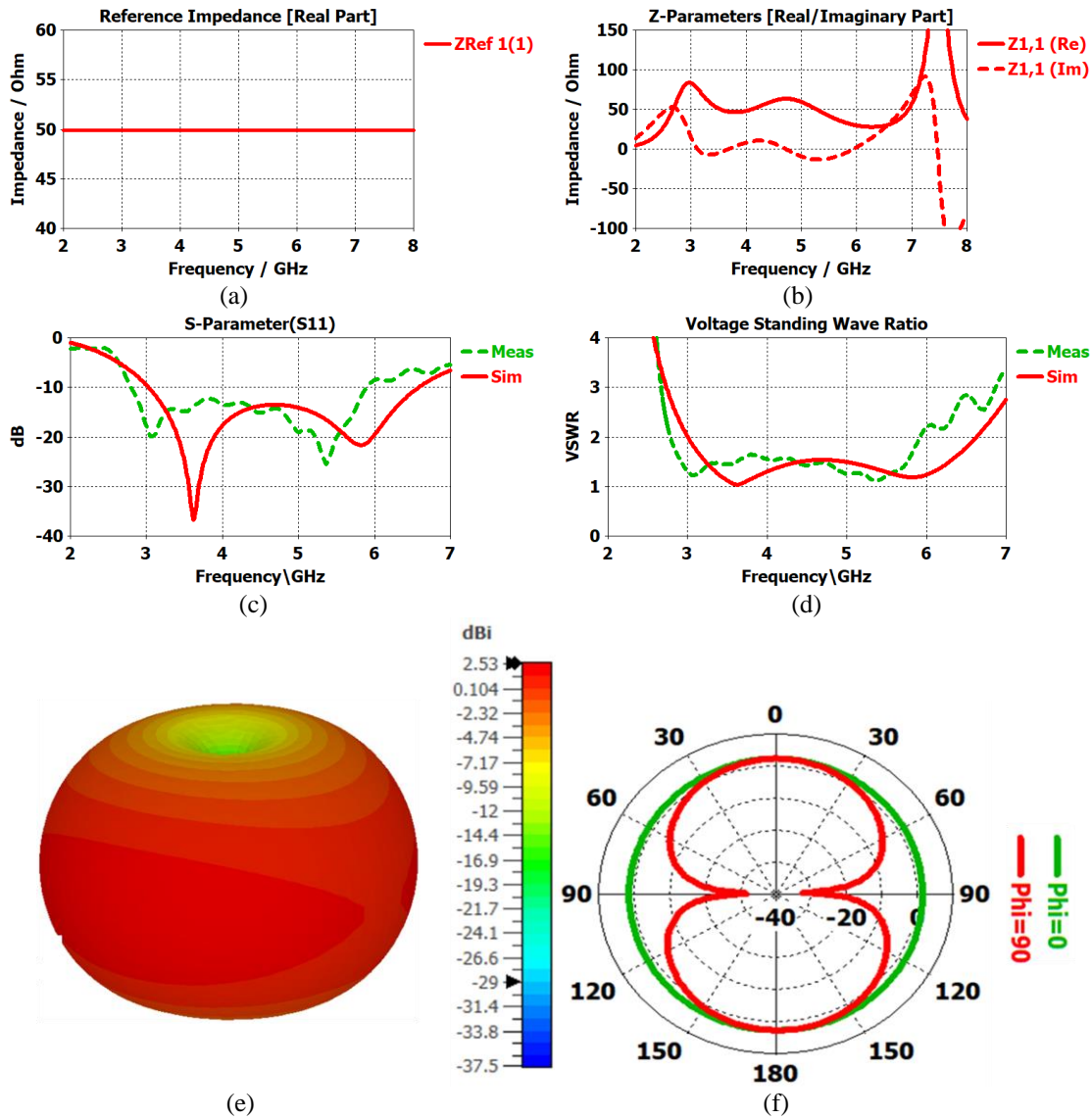


Figure. 5 Impedance, s-parameter, VSWR and radiation parameter of SEA design: (a) Reference impedance, (b) Real and imaginary impedance, (c) S_{11} , (d) VSWR, (e) 3-D radiation pattern, and (f) 2-D radiation pattern ($\phi = 0$ and $\phi = 90$)

MWS with the help of Eqs. (4) and (5) [19].

Here, $x = 1$, and $y = 2, 3, 4, 5$, and 6 . In theory, a lower ECC indicates better MIMO performance (MIMO standard in 0.4) [19]. From Fig. 7 (a), it is evident that the ECC value goes very low, around 0.0001, for most of the working BW of the design. At the beginning of the BW (2.82 GHz), the ECC is around 0.0025, and for the whole BW, the value never exceeds 0.004. In Fig. 7 (b), DG consistently stays around 10 throughout the bandwidth, never dropping below 9.98.

$$ECC_{xy} = \frac{|S_{xx}^* S_{xy} + S_{yx}^* S_{yy}|^2}{(1 - (|S_{xx}|^2 + |S_{xy}|^2))(1 - (|S_{xx}|^2 + |S_{yx}|^2))} \quad (4)$$

$$DG_{xy} = 10 \sqrt{1 - |ECC_{xy}|^2} \quad (5)$$

In Fig. 7 (c) and 7 (d), we observe MIMO antenna measurements in an anechoic chamber. Fig. 7(c) shows a 21% difference between measured and simulated peak TE, with the simulated reaching 92% and the measured value at 71%. This discrepancy may be due to fabrication or soldering. Similarly, the peak realized gain is 7 dBi (simulated) and 5.3 dBi (measured), possibly attributed to the same aforementioned factors.

Fig. 8 comprises the 3-D and 2-D radiation responses of the MIMO array. Here, only port 1 and port 2 have been chosen for measurement, as the other ports resemble them. Figs. 8 (a) and 8 (b) reveal the 3-D radiation pattern of port 1 and port 2, respectively. It is evident that at port 1, the 3-D pattern radiates mostly on the x-y plane, with some lower radiation strength points. To confirm the radiation characteristics, a 2-D analysis has been

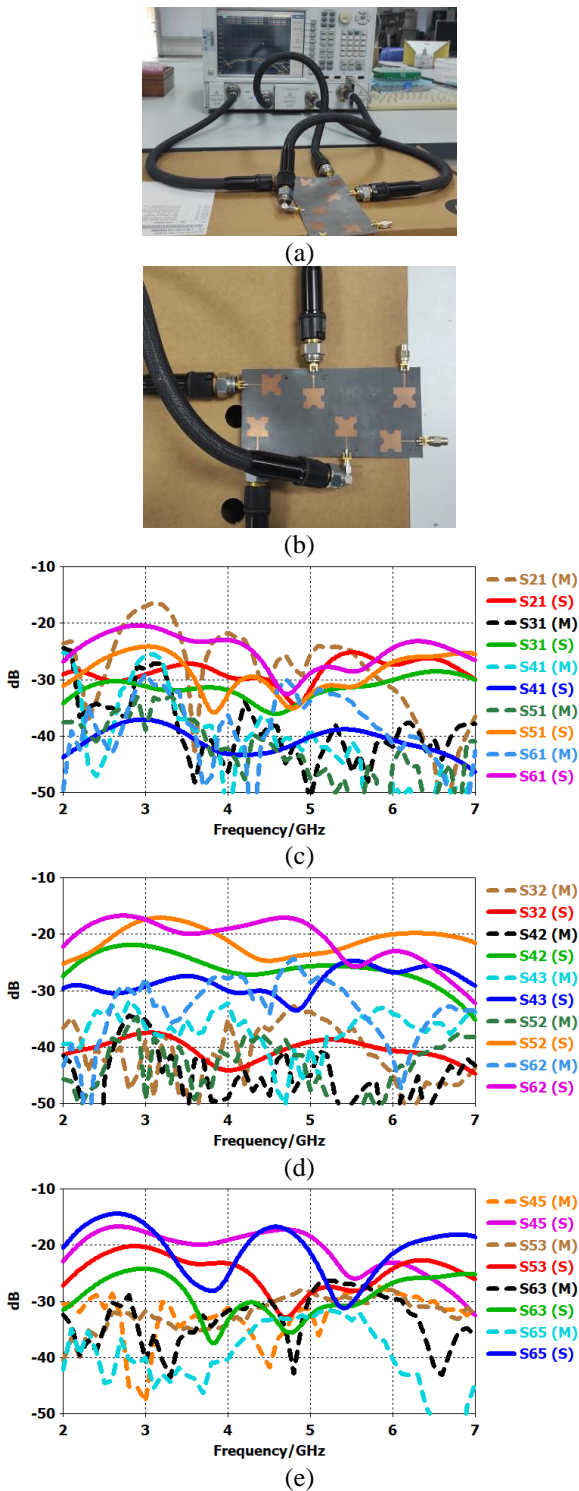


Figure. 6 Responses for the isolation between ports of MIMO design: (a) VNA measurement setup, (b) Connection at ports, (c), (d), and (e) Isolation between ports

done. Fig. 8 (c) reveals the 2-D radiation patterns (for $\Phi = 0^\circ$ and $\Phi = 90^\circ$). It is evident that, for both planes, the antenna radiates well and follows the 3-D pattern with less radiation at 0° and 180° degrees of the antenna plane. Similarly, we observe port 2's 3-D and 2-D radiation patterns in Figs. 8 (b)

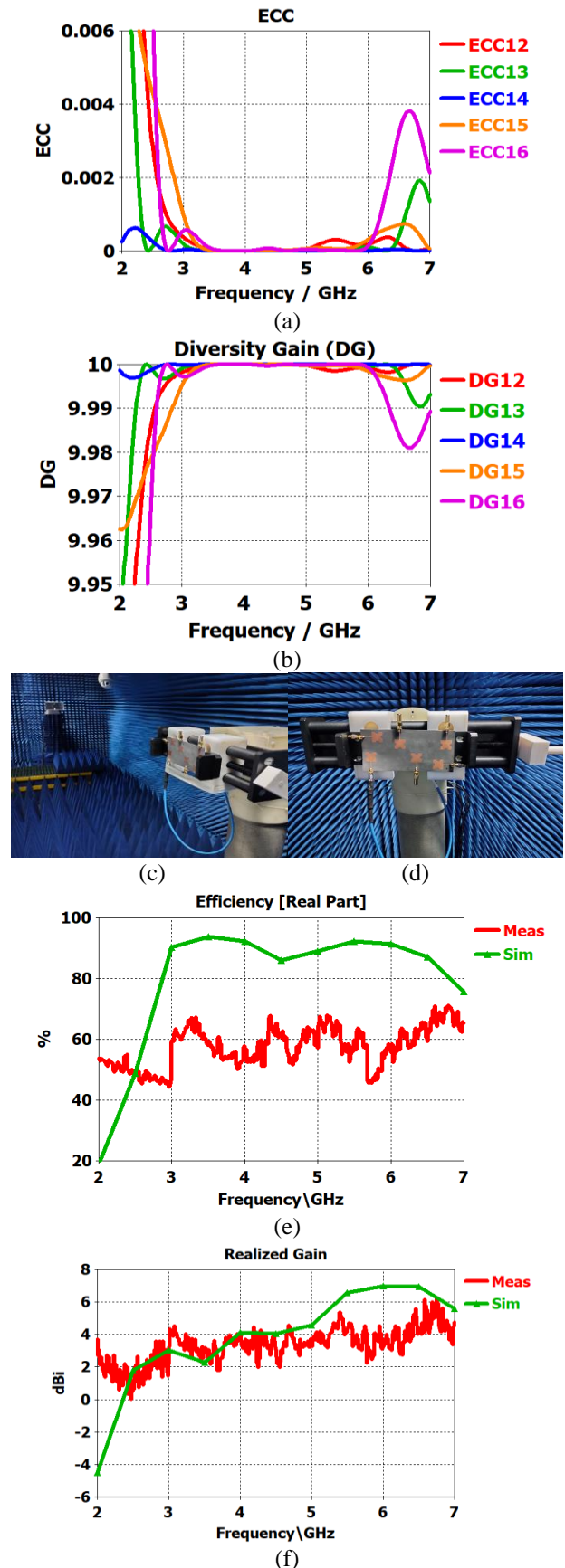


Figure. 7 The ECC, DG, Total antenna efficiency and the realized gain of the MIMO antenna: (a) ECC, (b) DG, (c) Anechoic chamber setup, (d) Antenna connection, (e) Total antenna efficiency, and (f) Realized gain

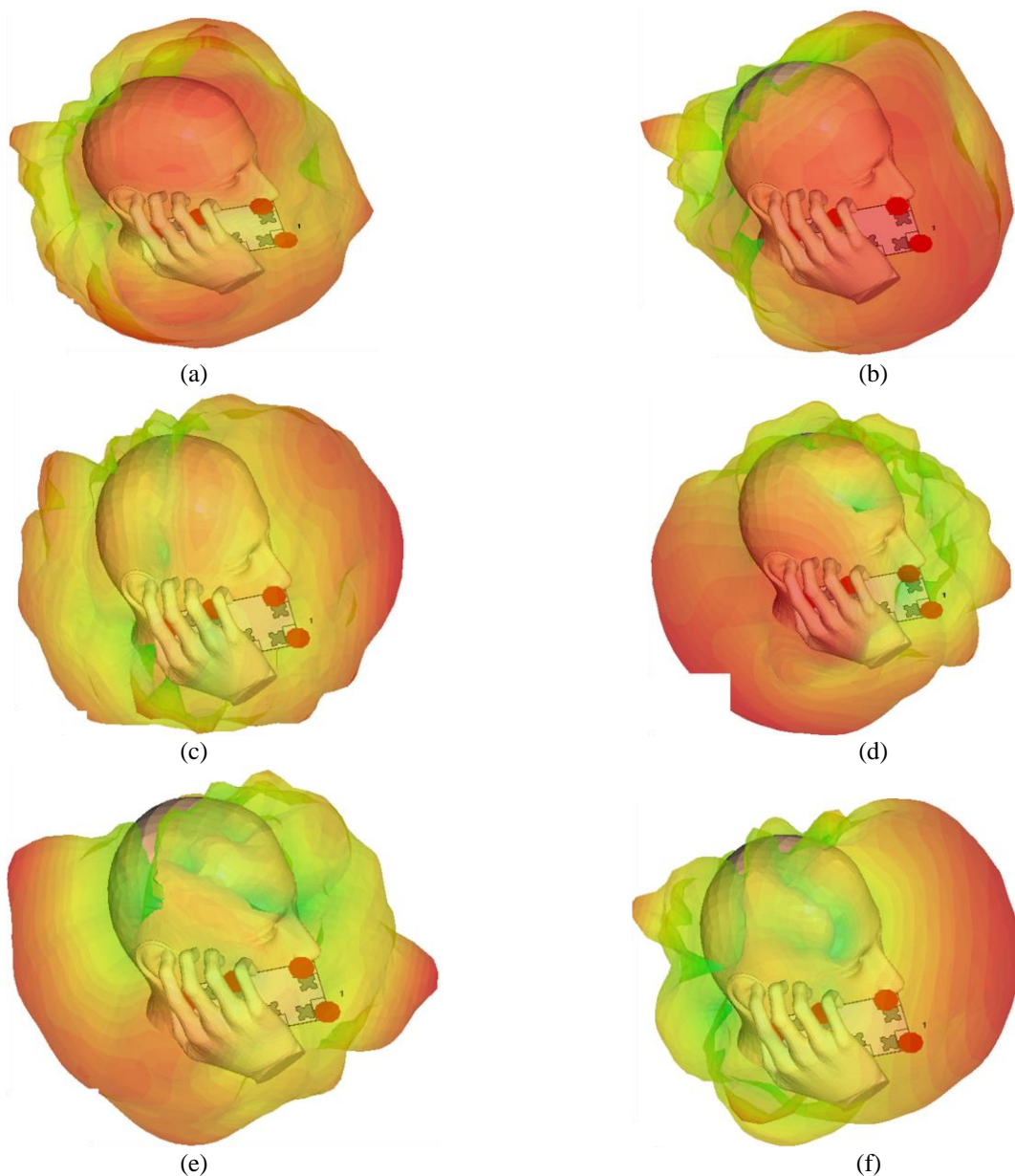


Figure. 9 The effect of hand-head phantom on radiation pattern: (a) port 1, (b) port 2, (c) port 3, (d) port 4, (e) port 5, and (f) port 6

and 8 (d), respectively. It is clear from the 3-D pattern that port 2 radiates the most on the y-z plane, with two nulls at 0 and 180 degrees of the antenna plane. The $\phi = 0^\circ$ and $\phi = 90^\circ$ 2-D radiation plots also confirm the same situation. After analyzing both port's radiation patterns, it can be said that the antenna can radiate in all directions, which is necessary for mobile communication.

Next, the same antenna has been exported and fitted inside a hand-head phantom model using CST MWS to analyze human interaction and the effect on the radiation pattern, as well as to calculate the SAR leaked into the head and hand of the human body. Figs. 9 and 10 reveal the responses of the 3-D radiation pattern and the SAR values, respectively, at 3.5 GHz for different ports. Figs. 9 (a) – 9 (f)

represent the 3-D radiation pattern responses for port 1 – port 6, respectively. It is observed that port 1, port 3, and port 6 radiate the beam in front of the head-hand phantom, while port 1, port 4, and port 5 radiate at the backside of the phantom. For each radiation pattern, it is clearly visible that the radiation is outwards from the hand-head, indicating low radiation power towards the body and less loss during communication between the mobile device and the nearest cell tower. Overall, it is also clear that the MIMO can communicate in all directions of the radiation.

Lastly, Figs. 10 (a) - 10 (f) represent the SAR responses for port 1 – port 6, respectively. The lowest SAR value is 0.13 W/Kg (port 1), and it goes as high as 0.78 W/Kg at port 5. For port 2, port 4,

port 3, and port 6, the SAR is 0.135 W/Kg, 0.154

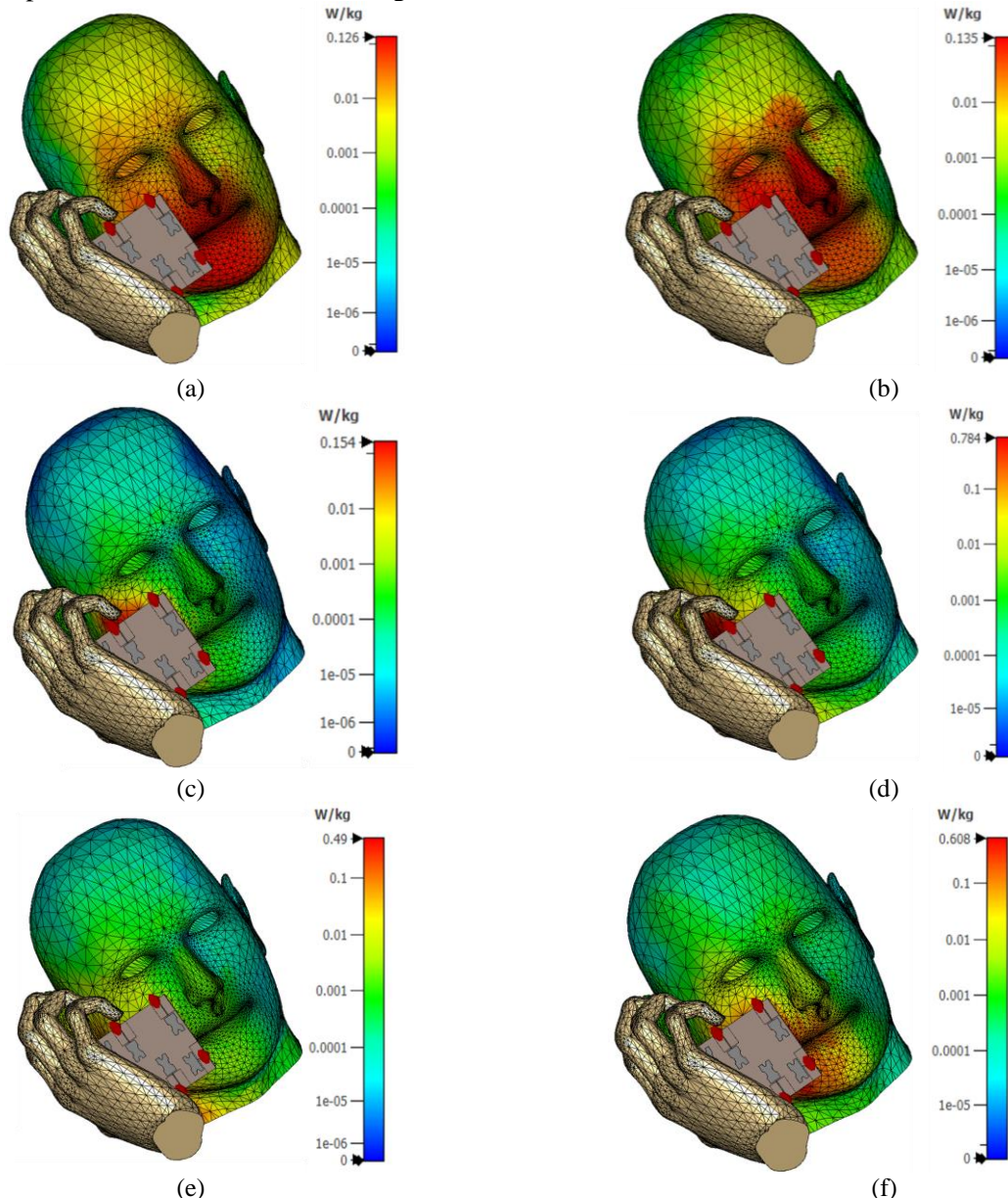


Figure. 10 SAR calculation with hand-head phantom using CST MWS: (a) port 1, (b) port 2, (c) port 3, (d) port 4, (e) port 5, and (f) port 6

W/Kg, 0.49 W/Kg, and 0.61 W/Kg, respectively. The standard for maximum SAR is 1.6 W/Kg and 2.0 W/Kg for 1g and 10g mass, respectively [5]. Based on this, it is evident that the SAR is well within the accepted standard and safe for use in smartphone communication for 5G.

4. Conclusions

This article presents a 6×6 MIMO array designed for sub-6 GHz mobile and wireless applications. The design's effectiveness is validated through both simulation and experimentation. Utilizing a partial ground plane (PGP), the array achieves a wideband response with 6 single-element

half-circle-slotted monopole antennas. The array's antennas are spaced 90 degrees apart to enable polarization diversity, and its dimensions of $75 \times 150 \text{ mm}^2$ make it suitable for integration into a 6.6-inch smartphone. Operating in the frequency range of 2.82 – 5.95 GHz, the array maintains a VSWR of less than 2 and offers a -10 dB bandwidth spanning approximately 3.13 GHz. It also achieves a minimum port-to-port isolation of less than -20 dB and a peak realized gain of 5.3 dBi, with an overall antenna efficiency of 71%. In terms of MIMO performance metrics, the ECC is consistently below 0.004, and the DG is at or above 9.98 across most of the operating bandwidth. Additionally, SAR testing confirms that the design meets safety and regulatory

standards, with values between 0.13-0.78 W/kg for a 10g mass.

Conflicts of interest

The authors declare no conflict of interest.

Author contributions

The authors' contributions are as follows: "Conceptualization, Fahmida Hossain and A K M Zakir Hossain; methodology, J. A. Jamil Alsayaydeh; software, Fahmida Hossain; validation, Muhammad Ibn Ibrahimy and J. A. Jamil Alsayaydeh; formal analysis Fahmida Hossain; investigation, Fahmida Hossain and A K M Zakir Hossain; resources, A K M Zakir Hossain; writing—original draft preparation, Fahmida Hossain and A K M Zakir Hossain; writing—review and editing, Muhammad Ibn Ibrahimy and funding acquisition, A K M Zakir Hossain.

Acknowledgments

This research has been funded by the fundamental research grant scheme (FRGS) with grant number of FRGS/1/2021/TK0/UTEM/02/34 provided by the Ministry of Higher Education Malaysia (MOHE) and managed by the Centre of Research and Innovation Management (CRIM), Universiti Teknikal Malaysia Melaka (UTeM).

References

- [1] A. Pant, M. Singh, and M. S. Parihar, "A frequency reconfigurable/switchable MIMO antenna for LTE and early 5G applications", *AEU - Int. J. Electron. Commun.*, Vol. 131, p. 153638, Mar. 2021, doi: 10.1016/J.AEUE.2021.153638.
- [2] J. Guo, L. Cui, C. Li, and B. Sun, "Side-Edge Frame Printed Eight-Port Dual-Band Antenna Array for 5G Smartphone Applications", *IEEE Trans. Antennas Propag.*, Vol. 66, No. 12, pp. 7412–7417, Dec. 2018, doi: 10.1109/TAP.2018.2872130.
- [3] N. Kumar and R. Khanna, "A two element MIMO antenna for sub-6 GHz and mmWave 5G systems using characteristics mode analysis", *Microw. Opt. Technol. Lett.*, Vol. 63, No. 2, pp. 587–595, Feb. 2021, doi: 10.1002/mop.32626.
- [4] A. A. Megahed, E. H. Abdelhay, M. Abdelazim, and H. Y. M. Soliman, "5G millimeter wave wideband MIMO antenna arrays with high isolation", *Eurasip J. Wirel. Commun. Netw.*, Vol. 2023, No. 1, 2023, doi: 10.1186/s13638-023-02267-y.
- [5] A. K. M. Z. Hossain, N. B. Hassim, W. H. W. Hassan, W. A. Indra, S. G. Herawan, and M. Z. A. B. A. Aziz, "A Planar 2×2 MIMO Antenna Array for 5G Smartphones", *Int. J. Adv. Comput. Sci. Appl.*, Vol. 12, No. 7, pp. 710–717, 2021, doi: 10.14569/IJACSA.2021.0120781.
- [6] Z. Ren and A. Zhao, "Dual-Band MIMO Antenna with Compact Self-Decoupled Antenna Pairs for 5G Mobile Applications", *IEEE Access*, Vol. 7, pp. 82288–82296, 2019, doi: 10.1109/ACCESS.2019.2923666.
- [7] J. Huang, G. Dong, J. Cai, H. Li, and G. Liu, "A Quad-Port Dual-Band MIMO Antenna Array for 5G Smartphone Applications", *Electron. 2021*, Vol. 10, No. 5, p. 542, 2021, doi: 10.3390/ELECTRONICS10050542.
- [8] M. A. Jamshed, M. U. Rehman, J. Frnda, A. A. Althwayb, A. Nauman, and K. Cengiz, "Dual Band and Dual Diversity Four-Element MIMO Dipole for 5G Handsets", *Sensors*, Vol. 21, No. 3, p. 767, 2021, doi: 10.3390/S21030767.
- [9] V. Yadav, R. S. Yadav, P. Yadav, B. Mishra, and A. Kumar, "Dual and wideband 6-port MIMO antenna for WiFi, LTE and carrier aggregation systems applications", *AEU - Int. J. Electron. Commun.*, Vol. 162, No. February, p. 154576, 2023, doi: 10.1016/j.aeue.2023.154576.
- [10] M. M. Morsy, "Compact eight-element MIMO antenna array for sub 6 GHz Mobile applications", *SN Appl. Sci.*, Vol. 5, No. 10, 2023, doi: 10.1007/s42452-023-05465-x.
- [11] N. O. Parchin et al., "An efficient antenna system with improved radiation for multi-standard/multi-mode 5G cellular communications", *Sci. Rep.*, Vol. 13, No. 1, pp. 1–15, 2023, doi: 10.1038/s41598-023-31407-z.
- [12] H. Ahmed, X. Zeng, H. Bello, Y. Wang, and N. Iqbal, "Sub-6 GHz MIMO antenna design for 5G smartphones: A deep learning approach", *AEU - Int. J. Electron. Commun.*, Vol. 168, p. 154716, 2023, doi: 10.1016/j.aeue.2023.154716.
- [13] Z. Wang, W. You, M. Yang, W. Nie, and W. Mu, "Design of MIMO Antenna with Double L-Shaped Structure for 5G NR", *Symmetry (Basel)*, Vol. 15, No. 3, 2023, doi: 10.3390/sym15030579.
- [14] M. Zahid, A. Khalid, H. Moazzam, H. Sadaqat, S. Shoaib, and Y. Amin, "Ten-Port MIMO Inverted-F Antenna for LTE Bands 43/48/49 Bands Smartphone Applications", *Electrics*, Vol. 12, No. 19, pp. 1–14, 2023, doi: 10.3390/electrics12194005.
- [15] J. P. Jhuang and H. L. Su, "A compact 12 × 12 MIMO loop antenna for 5G mobile phone

- applications”, *Int. J. Microw. Wirel. Technol.*, pp. 1–11, 2023, doi: 10.1017/S1759078723000673.
- [16] C. C. Lin, S. H. Cheng, S. C. Chen, and C. S. Wei, “Compact Sub 6 GHz Dual Band Twelve-Element MIMO Antenna for 5G Metal-Rimmed Smartphone Applications”, *Micromachines*, Vol. 14, No. 7, 2023, doi: 10.3390/mi14071399.
- [17] A. K. M. Z. Hossain, M. I. Ibrahimy, S. M. A. Motakabber, S. M. K. Azam, and M. S. Islam, “Multi-resonator application on size reduction for retransmission-based chipless RFID tag”, *Electron. Lett.*, Vol. 57, No. 1, pp. 26–29, 2021, doi: 10.1049/el12.12036.
- [18] M. S. Islam, A. K. M. Z. Hossain, and S. M. K. Azam, “Sequentially Rotated Four-Element Planar MIMO Array for 5G Cellular Communications”, In: *Proc. of 3rd IEEE Int. Virtual Conf. Innov. Power Adv. Comput. Technol. i-PACT 2021*, 2021, doi: 10.1109/I-PACT52855.2021.9696605.
- [19] A. K. M. Z. Hossain, M. I. Ibrahimy, T. Sutikno, M. H. Jopri, J. A. J. Alsayaydeh, and M. Manap, “A two-element planar multiple input multiple output array for ultra-wideband applications”, *Int. J. Electr. Comput. Eng.*, Vol. 12, No. 6, pp. 6847–6858, Dec. 2022, doi: 10.11591/IJECE.V12I6.PP6847-6858.